IOP Conf. Series: Journal of Physics: Conf. Series **1037** (2018) 032022 doi:10.1088/1742-6596/1037/3/032022

Detection of rotational periodic torque deviations in variable-speed wind turbine systems using disturbance observer and phase-locked loop

Korbinian Schechner[⋆], **Christoph M. Hackl**[⋆,†]

[⋆]MSE Research group "Control of Renewable Energy Systems (CRES)"
Technische Universität München, Lichtenbergstr. 4a, 85748 Garching
[†]Munich University of Applied Sciences, Lothstr. 64, 80335 Munich

E-mail: korbinian.schechner@tum.de

Abstract. We discuss the detection of rotational periodic torque deviations in variable speed wind turbine systems. These deviations can be caused by faults in the system. The turbine torque is estimated with an observer and an estimate of the ideal aerodynamical torque is calculated. These torques are analysed using a phase-locked loop to detect deviations. The torque observer is based on the model of the turbine drive train. It is modelled as a two-mass-system with a flexible shaft. The design of the observer and the phase-locked loop are shown and their stability is discussed. Simulations show, that the presented concept is capable of detecting the amplitude of the deviations at different periodicities, online and for variable speed.

Notation

$\mathbb{N}, \mathbb{R}, \mathbb{C}$: natural, real and complex numbers. $\mathbb{R}_{>\alpha} := (\alpha, \infty)$, ($\mathbb{R}_{\geq\alpha} := [\alpha, \infty)$): real numbers greater than (and equal to) $\alpha \in \mathbb{R}$. $\Re(s), \Im(s) \in \mathbb{R}$: real, imaginary part of $s \in \mathbb{C}$ with imaginary unit j. $\boldsymbol{x} := (x_1, \ldots, x_n)^\top \in \mathbb{R}^n$: column vector, $n \in \mathbb{N}$ where '$^\top$' and ':=' mean 'transposed' and 'is defined as'. $\mathrm{diag}(a_1, \ldots, a_n)$ in $\mathbb{R}^{n\times n}$: diagonal matrix with entries $a_1, \ldots, a_n \in \mathbb{R}$, $n \in \mathbb{N}$. $\boldsymbol{I}_n \in \mathbb{R}^{n\times n} := \mathrm{diag}(1, \ldots, 1)$: identity matrix. $\mathbf{0}_{n\times p} \in \mathbb{R}^{n\times p}$ zero matrix, $n, p \in \mathbb{N}$. $\xi \overset{(\#1)}{\underset{(\#2)}{=}} \zeta$: equivalence of ξ and ζ follows by invoking Eq. (#1) and Eq. (#2). $\boldsymbol{x} \in \mathbb{R}^n$ (in X)^n: physical quantity $\boldsymbol{x}$ where each of the n elements has SI-unit X. WhiteNoise is a function producing a signal with white noise distribution and maximal amplitude of 1.

1. Introduction

Condition monitoring and fault detection of wind turbines is an important task in the attempt of reducing failures and maintenance costs [1]. There is a huge variety of condition monitoring systems already available in the market. Most of the systems are based on vibration detection and require additional sensors and hardware installed in the wind turbine [2]. The purpose of these systems basically is to detect faults in the mechanical system of a wind turbine. Although stated to have relatively low costs (see [1]), the systems still cause additional expenses. To keep the costs of electricity—produced by wind turbine systems—at a minimum, while at the same time improving reliability of the system, condition monitoring techniques without the need of additional sensors seem to be an attractive choice.

There are several faults which not only cause vibrations in the components of a wind turbine, but also cause rotational periodic deviations on the turbine shaft torque m_T (in N m) (see [3]). So the turbine shaft torque can be represented as sum

$$m_T(t) := m_{T,\text{ideal}}(t) + m_{T,\text{dev}}(t), \tag{1}$$

of the ideal aerodynamical turbine torque $m_{T,\text{ideal}}$ (in N m) (caused by the wind speed on a fault-free wind turbine) and a deviation torque $m_{T,\text{dev}}$ (in N m). The deviation torque is the sum

$$m_{T,\text{dev}}(t) := \sum_r m_{T,\text{dev},r}(t) := \sum_r M_{T,\text{dev},r}(t) \cos\Big(\int_0^t r\,\omega_T(\tau)\mathrm{d}\tau + \varphi_{T,\text{dev},r,0}\Big), \quad r \in \mathbb{R}_{>0}. \tag{2}$$

of the rotational periodic torque deviations $m_{T,\text{dev},r}$ (in N m) with amplitude $M_{T,\text{dev},r}$ (in N m), r-th multiple ($r \in \mathbb{R}_{>0}$) of the turbine angular velocity ω_T ($\frac{\text{rad}}{\text{s}}$) and initial deviation angle $\varphi_{T,\text{dev},r,0}$ (in rad).
There are faults causing torque deviations for $r = 1$ (see [3], [4], [5], [6], [7]) like blade/shaft imbalance (e.g. due to icing), aerodynamic asymmetry (e.g. aged blades, unequal pitching of the blades, bended blades, defect blades) and partial damage in the magnets of a permanent magnet synchronous generator (at $r = \frac{1}{g_r}$, with gear box ratio g_r; only for direct drive systems at $r = 1$). Effects like yaw error, wind shear and tower shadow cause torque deviations with a multiple of $r = 3$ (see [8], [9]). There are torque deviations at other values of r as well. E.g. there are several faults for ball bearings resulting in different values of r depending on the number of balls, the diameter of inner and the outer race, etc. (see [3]).
There are two different detection approaches based on the analysed physical quantities. One directly analyses the torque signal. The other approach uses the machine currents. The idea behind the detection via the current is, that oscillations in the turbine torque also cause oscillations in the machine torque. As the machine torque is proportional to the machine currents, the oscillations are also visible in the machine currents. This approach is often chosen because the machine currents are usually measured; whereas the turbine torque is not measured, due to the high costs of torque sensors, see [1].
The publications [3], [4], [10], [11], [12], [13] use currents to detect faults in the wind turbine drive train. To overcome the problem of the missing torque sensor, these publications propose the use of an observer for the shaft torque of the turbine (see [14]), or use an observer for the aerodynamical torque cf. (4) (see [15], [16], [17]). The observed shaft torque is mostly used for fault detection. The aerodynamical torque is usually used for control purposes.
After obtaining signals—measured currents or observed torque—affected by the above mentioned faults, these signals need to be evaluated. The main technique to detect the periodic deviations given in (2), is the *Fourier Transform* (FT). Due to the varying turbine rotational speed ω_T, the Fourier Transform is not the best choice. So the *Short Time Fourier Transform* (STFT) or the *Wavelet Transform* (WT) are the standard methods for analysing the signals (see [2], [18], [19]). Both methods come with some disadvantages. To be able to work with variable frequencies, the STFT only takes the measurements of a time range in which the turbine speed is assumed to be constant. But due to the very slow rotation and the resulting oscillations with very low frequency, a wide time range is required to achieve an appropriate frequency resolution in the spectrum. But within this time range, ω_T is not constant any more. To overcome this time-frequency issue, the use of the WT is proposed (see [19], [20], [21], [22], [23]). But one significant disadvantage of WT is its long computation time, which makes online implementation quite challenging (see [22], [23]).
In view of the advantages and disadvantages of the available fault detection methods, we present in this paper a different approach. We combine a shaft torque observer with the calculation of the

(ideal) aerodynamical torque and the use of a *Phase-Locked Loop* (PLL) to analyse the signals to detect faults. The obtained amplitude of the torque deviation can be compared to a specific threshold to detect a fault. The proposed method is derived in detail and design guidelines are given.
The paper is organized as follows. First the modelling of a wind turbine system is presented focusing on the ideal aerodynamical torque and the turbine shaft torque. Based on these models, a disturbance observer for the wind turbine shaft torque is designed. To ease understanding, the working principle of a single-phase PLL and the design of its parameters is explained afterwards. Simulation results illustrate the capabilities and the properties of the proposed fault detection strategy for different experiments. A conclusion is drawn at the end.

2. Modelling of wind turbine system

This section describes the modelling of the considered wind turbine systems (aerodynamical modelling is based on [24]). Figure 1 shows a model of the corresponding wind turbine system. The extractable turbine power p_T (in W) can be calculated as

$$\begin{aligned} p_T(\lambda,\beta,v_W) &= c_P(\lambda,\beta)\, p_W(v_W) \\ &= c_P(\lambda,\beta)\tfrac{1}{2}\rho\pi r_T^2 v_W^3, \end{aligned} \tag{3}$$

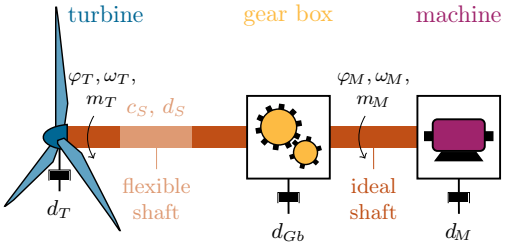

Figure 1: *Wind turbine system with flexible low speed shaft.*

based on air density ρ (in $\frac{\text{kg}}{\text{m}^3}$), turbine radius r_T (in m), wind speed v_W (in $\frac{\text{m}}{\text{s}}$) and a power coefficient $c_P(\lambda,\beta)$ which is a function of the tip speed ratio $\lambda := \frac{r_T\omega_T}{v_W}$ (depending on turbine radius r_T, turbine rotational speed ω_T (in $\frac{\text{rad}}{\text{s}}$) and wind speed v_W) and the pitch angle β (in °).

2.1. Modelling of turbine torque

Using (3) and the relation $p_T = m_T\omega_T$ the ideal (caused by the wind speed v_W on a perfectly working wind turbine) turbine torque $m_{T,\text{ideal}}$ (in N m) can be calculated as

$$m_{T,\text{ideal}}(\lambda,\beta,\omega_T) := \tfrac{p_T(\lambda,\beta,v_W)}{\omega_T} \overset{(3)}{=} \tfrac{1}{2}\rho\pi r_T^2 v_W^3 \tfrac{c_P(\lambda,\beta)}{\omega_T} = \tfrac{1}{2}\rho\pi r_T^5 \tfrac{c_P(\lambda,\beta)}{\lambda^3}\omega_T^2. \tag{4}$$

2.2. Drive train modelling

The wind turbine's drive train is modelled as two-mass system with high speed shaft and low speed shaft (see Fig. 1, [25, Chap. 12]). The dynamics of such a flexible TMS are given by the following nonlinear third-order state-space model

$$\left.\begin{aligned} \tfrac{\mathrm{d}}{\mathrm{d}t}\boldsymbol{x}(t) &= \boldsymbol{A}\boldsymbol{x}(t) + \boldsymbol{b}u(t) + \boldsymbol{b}_d d(t) \\ \boldsymbol{y}(t) &= \boldsymbol{C}\boldsymbol{x}(t) \end{aligned}\right\} \tag{5}$$

where

$$\left.\begin{aligned} \boldsymbol{x}(t) &= \begin{pmatrix} \omega_T(t) \\ \omega_M(t) \\ \Delta\varphi_{TM'}(t) \end{pmatrix}, \quad u(t) = m_M(t), \quad d(t) = m_T(t), \quad \boldsymbol{b} = \begin{pmatrix} 0 \\ \frac{1}{\Theta_M+\Theta_{Gb}} \\ 0 \end{pmatrix}, \\ \boldsymbol{A} &= \begin{bmatrix} -\frac{d_S+d_T}{\Theta_T} & \frac{d_S}{g_r\Theta_T} & -\frac{c_S}{\Theta_T} \\ \frac{d_S}{g_r(\Theta_M+\Theta_{Gb})} & -\frac{d_S+g_r^2(d_M+d_{Gb})}{g_r^2(\Theta_M+\Theta_{Gb})} & \frac{c_S}{g_r(\Theta_M+\Theta_{Gb})} \\ 1 & -\frac{1}{g_r} & 0 \end{bmatrix}, \quad \boldsymbol{b}_d = \begin{pmatrix} \frac{1}{\Theta_T} \\ 0 \\ 0 \end{pmatrix}, \quad \boldsymbol{C} = \begin{bmatrix} 1 & 0 & 0 \\ 0 & 1 & 0 \\ 0 & 0 & 1 \end{bmatrix} \end{aligned}\right\} \tag{6}$$

are the state vector $\boldsymbol{x} \in \mathbb{R}^3$, input $u \in \mathbb{R}$, disturbance $d \in \mathbb{R}$, output vector $\boldsymbol{y} \in \mathbb{R}^3$, state matrix $\boldsymbol{A} \in \mathbb{R}^{3\times3}$, input vector $\boldsymbol{b} \in \mathbb{R}^3$, disturbance input vector $\boldsymbol{b}_d \in \mathbb{R}^3$ and output matrix $\boldsymbol{C} \in \mathbb{R}^{3\times3}$. The initial values of the state vector are given by $\boldsymbol{x}(0) = (\omega_{T,0}, \omega_{M,0}, \varphi_{TM',0})^\top \in \mathbb{R}^3$ (in $(\frac{\text{rad}}{\text{s}}, \frac{\text{rad}}{\text{s}}, \text{rad})^\top$). The physical quantities in (6) represent turbine inertia Θ_T (in $\text{kg}\,\text{m}^2$), gear box inertia Θ_{Gb} (in $\text{kg}\,\text{m}^2$), machine inertia Θ_M (in $\text{kg}\,\text{m}^2$), turbine damping d_T (in $\frac{\text{N}\,\text{m}\,\text{s}}{\text{rad}}$), gear box damping d_{Gb} (in $\frac{\text{N}\,\text{m}\,\text{s}}{\text{rad}}$), machine damping d_M (in $\frac{\text{N}\,\text{m}\,\text{s}}{\text{rad}}$), shaft damping d_S (in $\frac{\text{N}\,\text{m}\,\text{s}}{\text{rad}}$), shaft stiffness c_S (in $\frac{\text{N}\,\text{m}}{\text{rad}}$), turbine rotational speed ω_T (in $\frac{\text{rad}}{\text{s}}$), machine rotational speed ω_M (in $\frac{\text{rad}}{\text{s}}$), turbine torque m_T (in $\text{N}\,\text{m}$), machine torque m_M (in $\text{N}\,\text{m}$), angle of twist $\varphi_{TM'} := \int(\omega_T - \frac{1}{g_r}\omega_M)\text{d}t + \varphi_{TM',0}$ (in rad), turbine rotational speed initial value $\omega_{T,0}$ (in $\frac{\text{rad}}{\text{s}}$), machine rotational speed initial value $\omega_{M,0}$ (in $\frac{\text{rad}}{\text{s}}$) and initial torsion angle $\varphi_{TM',0}$ (in rad).

3. Observation of turbine torque

In modern wind turbine systems usually the three states, ω_T, ω_M and $\Delta\varphi_{TM'}$ are measured (actually $\Delta\varphi_{TM'}$ is calculated using the measured machine angle φ_M and turbine angle φ_T). The machine torque is known due to its reference value, see (A.1). But the turbine torque is usually unknown, because there is no torque sensor used in wind turbine drive trains (e.g. due to the high price). So an observer has to be derived to estimate the turbine torque m_T. To determine the turbine torque the machine torque is needed. Therefore, we impose the following assumption:

Assumption (A.1) *The machine torque m_M equals*[1] *the reference torque $m_{M,\text{ref}}$ (in $\text{N}\,\text{m}$), i.e.*

$$m_M(t) = m_{M,\text{ref}}(t), \quad \forall t \geq 0. \tag{7}$$

The time delay between $m_{M,\text{ref}}$ (demanded by the control system) and the actual machine torque m_M is neglected because of the much faster dynamics of the electrical machine compared to the mechanical dynamics of the turbine or the two-mass system.

3.1. Augmented system model

To create a disturbance observer, an augmented system with an additional virtual state x_d (in $\text{N}\,\text{m}$) representing the disturbance is necessary (variables with $^\wr$ represent augmented variables due to the changed system). The disturbance d is spilt up into a constant value d_0 and a changing value $\overline{d}$

$$\left.\begin{array}{rcl} \frac{\text{d}}{\text{d}t}\boldsymbol{x}^\wr(t) & = & \boldsymbol{A}^\wr\boldsymbol{x}^\wr(t) + \boldsymbol{b}^\wr u(t) + \boldsymbol{b}_d^\wr\overline{d}(t) \\ \boldsymbol{y}(t) & = & \boldsymbol{C}^\wr\boldsymbol{x}^\wr(t) \end{array}\right\} \tag{8}$$

with $\frac{\text{d}}{\text{d}t}x_d(t) = 0$ and initial value $x_d(0) = d_0$

$$\left.\begin{array}{c} \boldsymbol{x}^\wr(t) := \begin{pmatrix}\boldsymbol{x}(t)\\ x_d(t)\end{pmatrix}, \quad u(t) = m_M(t), \quad d(t) = d_0 + \overline{d}(t) = m_T(t) \\ \boldsymbol{A}^\wr := \begin{bmatrix}\boldsymbol{A} & \boldsymbol{b}_d\\ \boldsymbol{0}_{1\times4}\end{bmatrix}, \quad \boldsymbol{b}^\wr := \begin{pmatrix}\boldsymbol{b}\\ 0\end{pmatrix}, \quad \boldsymbol{b}_d^\wr := \begin{pmatrix}\boldsymbol{b}_d\\ 0\end{pmatrix}, \quad \boldsymbol{C}^\wr := \begin{bmatrix}\boldsymbol{C} & \boldsymbol{0}_{3\times1}\end{bmatrix}. \end{array}\right\} \tag{9}$$

3.2. Disturbance observer

To implement an observer, the system (8) has to be observable. To test observability, the matrix $\boldsymbol{Q}^\wr := [(\boldsymbol{C}^\wr)^\top, (\boldsymbol{C}^\wr\boldsymbol{A}^\wr)^\top, (\boldsymbol{C}^\wr{\boldsymbol{A}^\wr}^2)^\top, (\boldsymbol{C}^\wr{\boldsymbol{A}^\wr}^3)^\top]^\top \in \mathbb{R}^{12\times4}$ must have full rank. Since $\frac{1}{\Theta_T} \neq 0$, it becomes apparent that $\text{rank}(\boldsymbol{Q}^\wr) = 4$. Hence, system (8) is observable.

[1] This implies a perfectly working torque control. If this assumption does not hold, this might impact wind turbine efficiency and power production, [26].

The state equations of the observer can be summarized as follows

$$\left.\begin{array}{rcl} \frac{\mathrm{d}}{\mathrm{d}t}\hat{\boldsymbol{x}}^{\wr}(t) &=& \boldsymbol{A}^{\wr}\hat{\boldsymbol{x}}^{\wr}(t) + \boldsymbol{b}^{\wr}u(t) + \boldsymbol{L}^{\wr}\left(\boldsymbol{y}(t) - \hat{\boldsymbol{y}}(t)\right) \\ \hat{\boldsymbol{y}}(t) &=& \boldsymbol{C}^{\wr}\hat{\boldsymbol{x}}^{\wr}(t), \quad \hat{y}_d^{\wr}(t) = {\boldsymbol{c}_d^{\wr}}^{\top}\hat{\boldsymbol{x}}^{\wr}(t). \end{array}\right\} \tag{10}$$

Variables with $\hat{}$ are observed values. $\boldsymbol{L}^{\wr}$ is the observer gain matrix, ${\boldsymbol{c}_d^{\wr}}^{\top} := (0,0,0,1)$ the disturbance observation vector and $\hat{y}_d^{\wr} \in \mathbb{R}$ the output for the observed disturbance, so $\hat{y}_d^{\wr} \approx \overline{d}$. A block diagram of the system and the observer is shown in Fig. 2.

To choose the values of the observer gain matrix $\boldsymbol{L}^{\wr}$, the linear quadratic regulator (LQR) approach is chosen, see [27, pp. 220-224] or [28, pp. 511-513]. For linear quadratic regulator design, the dual system

$$\left.\begin{array}{l} \frac{\mathrm{d}}{\mathrm{d}t}\boldsymbol{x}_{\diamond}^{\wr}(t) = {\boldsymbol{A}^{\wr}}^{\top}\boldsymbol{x}_{\diamond}^{\wr}(t) + {\boldsymbol{C}^{\wr}}^{\top}\boldsymbol{u}_{\diamond}^{\wr}(t), \\ \boldsymbol{u}_{\diamond}^{\wr}(t) = -{\boldsymbol{L}^{\wr}}^{\top}\boldsymbol{x}_{\diamond}^{\wr}(t) \end{array}\right\} \tag{11}$$

with dual state $\boldsymbol{x}_{\diamond}^{\wr}$, its initial value $\boldsymbol{x}_{\diamond}^{\wr}(0) = \boldsymbol{x}_{\diamond,0}^{\wr}$ and dual input $\boldsymbol{u}_{\diamond}^{\wr}$ is used. The property $\det\left({\boldsymbol{A}^{\wr}}^{\top} - {\boldsymbol{C}^{\wr}}^{\top}{\boldsymbol{L}^{\wr}}^{\top}\right) = \det\left(\boldsymbol{A}^{\wr} - \boldsymbol{L}^{\wr}\boldsymbol{C}^{\wr}\right)$ ensures the same stability behaviour as for the original system, see [28, Sect. 13.7.2].

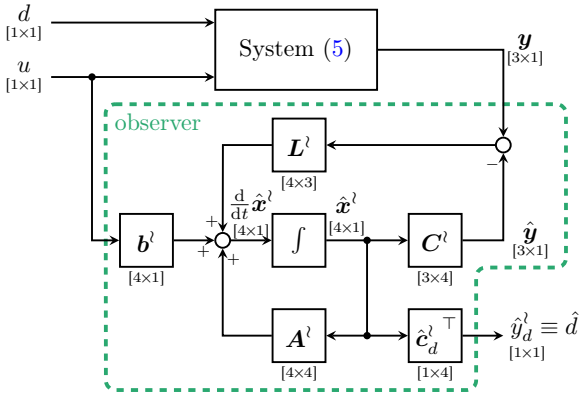

Figure 2: *Block diagram of system (5) with observer (10).*

The LQR design minimizes the cost function $J = \int_0^{\infty} \mathrm{e}^{2\alpha t}\left(\boldsymbol{x}_{\diamond}^{\wr}(t)^{\top}\boldsymbol{Q}\boldsymbol{x}_{\diamond}^{\wr}(t) + \boldsymbol{u}_{\diamond}^{\wr}(t)^{\top}\boldsymbol{R}\boldsymbol{u}_{\diamond}^{\wr}(t)\right)\mathrm{d}t$ with stability margin $\alpha \geq 0$ and weighting matrices $0 \leq \boldsymbol{Q} = \boldsymbol{Q}^{\top} \in \mathbb{R}^{4\times4}$ and $0 < \boldsymbol{R} = \boldsymbol{R}^{\top} \in \mathbb{R}^{3\times3}$. For given $\boldsymbol{Q}$ and $\boldsymbol{R}$, the observer-gain matrix can be calculated as $\boldsymbol{L}^{\wr} = \boldsymbol{P}{\boldsymbol{C}^{\wr}}^{\top}\boldsymbol{R}^{-1}$ where $0 < \boldsymbol{P} = \boldsymbol{P}^{\top} \in \mathbb{R}^{4\times4}$ is the solution of the Riccati-equation $\boldsymbol{0}_{4\times4} = \left(\boldsymbol{A}^{\wr} + \alpha\boldsymbol{I}_4\right)\boldsymbol{P} + \boldsymbol{P}\left(\boldsymbol{A}^{\wr} + \alpha\boldsymbol{I}_4\right)^{\top} + \boldsymbol{Q} - \boldsymbol{P}{\boldsymbol{C}^{\wr}}^{\top}\boldsymbol{R}^{-1}\boldsymbol{C}^{\wr}\boldsymbol{P}$. Is the system with $\boldsymbol{A}^{\wr} + \alpha\boldsymbol{I}_4$ and $\boldsymbol{C}^{\wr}$ observable, all poles of the observer have a real part with at least $-\alpha$, see [27, Sect. 10.4.5]. To ensure observability of the system (10) with gain $\boldsymbol{L}^{\wr}$ and stability margin α, $\boldsymbol{Q}_{\alpha}^{\wr} := [(\boldsymbol{C}^{\wr})^{\top}, (\boldsymbol{C}^{\wr}(\boldsymbol{A}^{\wr} + \alpha\boldsymbol{I}_4))^{\top}, (\boldsymbol{C}^{\wr}(\boldsymbol{A}^{\wr} + \alpha\boldsymbol{I}_4)^2)^{\top}, (\boldsymbol{C}^{\wr}(\boldsymbol{A}^{\wr} + \alpha\boldsymbol{I}_4)^3)^{\top}]^{\top} \in \mathbb{R}^{12\times4}$ must have full rank. Again (see observability of original system (6)), since $\frac{1}{\Theta_T} \neq 0$ the extended system with $\boldsymbol{A}^{\wr} + \alpha\boldsymbol{I}_4$ and $\boldsymbol{C}^{\wr}$ is observable.

4. Single phase phase-locked loop (PLL)

Phase-locked loops are applied in many fields. They are used for tracking filters, frequency synthesis, clock synchronization, frequency and phase demodulation, etc. (see [29]). In power grids three-phase PLLs are applied. In order to detect the deviations in the observed torque of the wind turbine, a single-phase phase-locked loop will be used. Figure 3 shows the structure and the parts of the applied PLL. This section explains the functionality of the PLL and its tuning for torque deviation detection.

The PLL uses a Park-transform-based quadrature signal generator (QSG) to create the signal $v^{\beta,\bullet}$ (in X) which is perpendicular to input $v = v^{\alpha}$ (in X) (with arbitrary SI-unit X). For that, the Park transform $\boldsymbol{T}_P(\phi) := \begin{bmatrix}\cos(\phi) & -\sin(\phi) \\ \sin(\phi) & \cos(\phi)\end{bmatrix}$ and its inverse $\boldsymbol{T}_P^{-1}(\phi) := \begin{bmatrix}\cos(\phi) & \sin(\phi) \\ -\sin(\phi) & \cos(\phi)\end{bmatrix}$ with angle ϕ (in rad) are employed . The inverse Park transform transforms stationary (sinusoidal) signals $\boldsymbol{\xi}^{\alpha\beta} := (\xi^{\alpha}, \xi^{\beta})^{\top}$ (in X)^2 into constant signals $\boldsymbol{\xi}^{dq} := (\xi^{d}, \xi^{q})^{\top} := \boldsymbol{T}_P^{-1}(\phi)\boldsymbol{\xi}^{\alpha\beta}$ (in X)^2 in

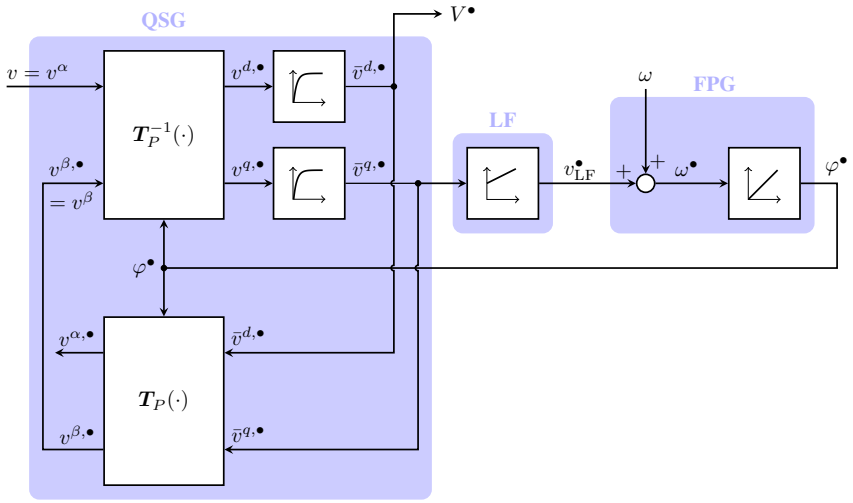

Figure 3: *Phase-locked loop based on inverse Park transform (based on [30, Figure 4]). It consists of three components: quadrature signal generator (QSG), loop filter (LF) and the frequency/phase-angle generator (FPG) which provides the phase angle for the QSG.*

the synchronously rotating d-q-reference frame. The Park transform does vice-versa. For the functionality of the QSG, a first-order low-pass filter

$$\frac{\mathrm{d}}{\mathrm{d}t}\bar{v}^{d/q,\bullet}(t) = \frac{1}{T_F}\left(v^{d/q,\bullet}(t) - \bar{v}^{d/q,\bullet}(t)\right), \quad \bar{v}^{d/q,\bullet}(0) = \bar{v}_0^{d/q,\bullet} \tag{12}$$

with filter time constant T_F (in s) or filter frequency ω_f (in $\frac{1}{\mathrm{s}}$) and transfer function

$$F(s) = \frac{\bar{v}^{d/q,\bullet}(s)}{v^{d/q,\bullet}(s)} = \frac{1}{1+sT_F} = \frac{\omega_f}{\omega_f + s} \quad \text{with} \quad T_F = \frac{1}{\omega_f} \tag{13}$$

is necessary, see Sect. 4.2.1 and [30]. It filters the identified values $v^{d,\bullet}$ (in X) and $v^{q,\bullet}$ (in X). The resulting values are $\bar{v}^{d,\bullet}$ (in X) and $\bar{v}^{q,\bullet}$ (in X) with initial values $\bar{v}_0^{d,\bullet}$ (in X) and $\bar{v}_0^{q,\bullet}$ (in X), respectively.

4.1. Small signal approximation of QSG

Based on the overall system parameters the gains of the PI controller of the PLL (loop filter (LF) in Fig. 3) and the filter frequency ω_f will be chosen. For that a small signal approximation of the PLL will be performed (for more details see [30] and [31, Sect. 4.4]). To do so the following assumptions are imposed.

Assumption (A.2) *The input signal v (in X) of the PLL is a cosine signal, i.e.*

$$v(t) = V(t)\cos\left(\varphi(t)\right), \text{ where } \varphi(t) := \int_0^t \omega(\tau)\mathrm{d}\tau + \varphi_0 \tag{14}$$

with positive but time-varying amplitude V (in X), angular velocity ω (in $\frac{\mathrm{rad}}{\mathrm{s}}$), angle φ (in rad*) and its initial value φ_0 (in* rad*).*

Assumption (A.3) *The QSG works ideally, i.e.*

$$v(t) = V(t)\cos(\varphi(t)) = v^\alpha(t) \tag{15}$$

$$v^{\beta,\bullet}(t) = V(t)\cos\left(\varphi(t) - \tfrac{\pi}{2}\right) = V(t)\sin(\varphi(t)) = v^\beta(t), \tag{16}$$

so $v^{\beta,\bullet}$ is rotated by 90° with respect to v.

Assumption (A.4) *The PLL works already close to the correct value, i.e.* $\varphi^\bullet(t) \approx \varphi(t)$ *and hence* $\cos(\varphi^\bullet(t) - \varphi(t)) \approx 1$ *and* $\sin(\varphi(t) - \varphi^\bullet(t)) \approx \varphi(t) - \varphi^\bullet(t)$.
Assumption (A.5) *The amplitude of the input signal is* $V(t) = 1$ *(or was normalized a priori).*

Combining (A.2) and (A.3), $\boldsymbol{v}^{\alpha\beta}$ can be expressed as

$$\boldsymbol{v}^{\alpha\beta}(t) = \begin{pmatrix} v^\alpha(t) \\ v^\beta(t) \end{pmatrix} \overset{(A.3)}{=} \begin{pmatrix} v(t) \\ v^{\beta,\bullet}(t) \end{pmatrix} \underset{(A.3)}{\overset{(A.2)}{=}} \begin{pmatrix} V(t)\cos(\varphi(t)) \\ V(t)\sin(\varphi(t)) \end{pmatrix}. \tag{17}$$

This results in

$$\boldsymbol{v}^{dq,\bullet}(t) = \boldsymbol{T}_P^{-1}(\varphi^\bullet(t))\boldsymbol{v}^{\alpha\beta}(t) \overset{(17)}{=} V(t) \begin{pmatrix} \cos(\varphi^\bullet(t) - \varphi(t)) \\ \sin(\varphi(t) - \varphi^\bullet(t)) \end{pmatrix}. \tag{18}$$

Using Assumptions (A.4) and (A.5), this relation simplifies to

$$\boldsymbol{v}^{dq,\bullet}(t) \underset{(18)}{\overset{(A.4)}{=}} V(t) \begin{pmatrix} 1 \\ \varphi(t) - \varphi^\bullet(t) \end{pmatrix} \overset{(A.5)}{=} \begin{pmatrix} 1 \\ \varphi(t) - \varphi^\bullet(t) \end{pmatrix}. \tag{19}$$

Remark 4.1. *Assumption (A.5) is crucial. For the PLL to lock, the output of the quadrature signal generator (QSG) has to be normalized. For this at least the dimension of the wanted amplitude should be known and used for normalization. For fault detection e.g. the limit of the amplitude for indicating a fault could be used. A flexible normalization of the q-component* $v^{q,\bullet}$ *with the norm of the vector* $\left\|\boldsymbol{v}^{dq,\bullet}\right\|$*, as used in [24] is not advisable here. For the fault free case the norm* $\left\|\boldsymbol{v}^{dq,\bullet}\right\|$ *is zero and one would divide* $v^{q,\bullet}$ *by zero.*

For the q-component $v^{q,\bullet}$ in (19) (see Fig. 3), the small-signal block diagram of the PLL is depicted in Fig. 4.

4.2. Determination of PLL parameter

The parameter of the PLL—filter time constant and proportional and integral gain of the PI controller—will be designed applying a parameter based approach. For that, the small signal approximation of the PLL in Fig. 4 is used.

4.2.1. Determination of filter time constant A DC-component in the signal v will result in an oscillation in $\boldsymbol{v}^{dq,\bullet}$ with the frequency of $\omega^\bullet$ (see Fig. 3). To damp these oscillations, the low pass filter is used (see [30]). Since the desired damping is also required for the minimal rotational frequency $\omega_{\min,r}$ (in $\frac{\text{rad}}{\text{s}}$), we chose the filter frequency ω_f as follows

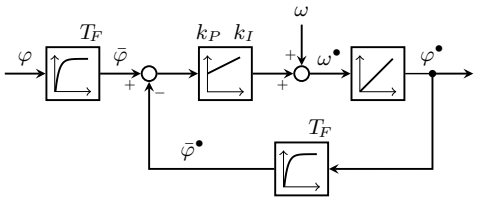

Figure 4: *Small-signal block diagram of PLL.*

$$\omega_f = \sqrt{\frac{\left|F_{v^{d/q,\bullet}\to\bar{v}^{d/q,\bullet}}(j\omega_{\min,r})\right|^2\omega_{\min,r}^2}{1-\left|F_{v^{d/q,\bullet}\to\bar{v}^{d/q,\bullet}}(j\omega_{\min,r})\right|^2}} = \sqrt{\frac{\left(10^{\frac{\left|F_{v^{d/q,\bullet}\to\bar{v}^{d/q,\bullet}}(j\omega_{\min,r})\right|_{\text{dB}}}{20}}\right)^2\omega_{\min,r}^2}{1-\left(10^{\frac{\left|F_{v^{d/q,\bullet}\to\bar{v}^{d/q,\bullet}}(j\omega_{\min,r})\right|_{\text{dB}}}{20}}\right)^2}} \tag{20}$$

with

$$F_{v^{d/q,\bullet}\to\bar{v}^{d/q,\bullet}}(j\omega_{\min,r}) \overset{(13)}{=} \frac{\omega_f}{\omega_f + j\omega_{\min,r}} = \frac{\omega_f^2 - j\omega_{\min,r}\omega_f}{\omega_f^2 + \omega_{\min,r}^2}. \tag{21}$$

So ω_f depends on the desired damping $\left|F_{v^{d/q,\bullet}\to\bar{v}^{d/q,\bullet}}(j\omega_{\min,r})\right|_{\text{dB}}$ at the minimal frequency $\omega_{\min,r}$. Depending on the rotational periodicity r of the torque deviation and the minimal rotational speed $\omega_{T,\min}$ of the turbine, the minimal frequency $\omega_{\min,r}$ of the PLL has to be chosen accordingly i.e. $\omega_{\min,r} := r\omega_{T,\min}$, which is a turbine specific parameter.

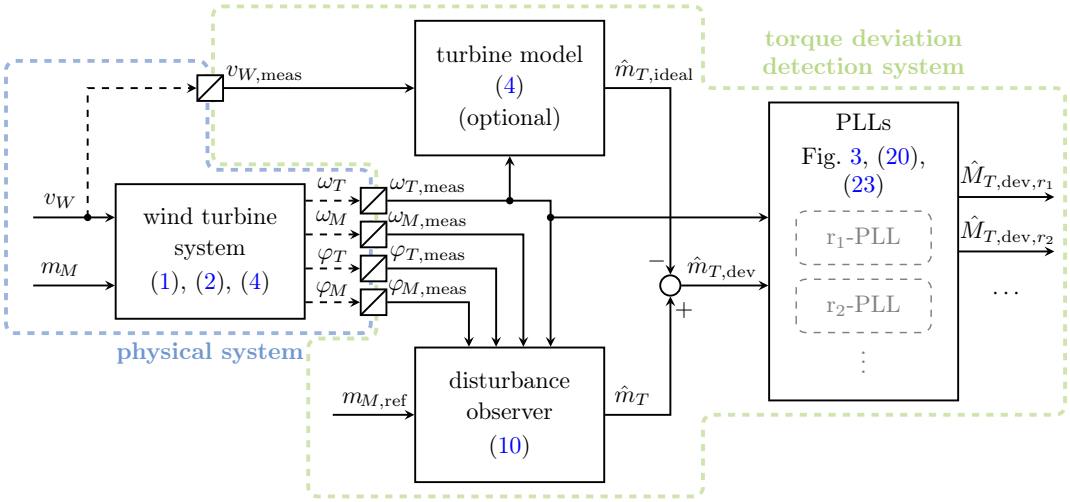

Figure 5: *Implementation of the torque deviation detection system.*

4.2.2. Determination of PI controller parameter The small-signal system shown in Fig. 4 can be seen as the combination of an integrator and a first-order lag system with transfer function

$$F_{\omega^\bullet \to \bar{\varphi}^\bullet}(s) = \frac{\bar{\varphi}^\bullet(s)}{\omega^\bullet(s)} = \frac{1}{s}\frac{1}{1+sT_F} = \frac{1}{s\left(1+s\frac{1}{\omega_f}\right)}. \tag{22}$$

Based on the symmetrical optimum, the parameters of the PI-controller can be determined (see [32, Chap. 3]) as follows $k_P = \frac{1}{2T_F} = \frac{\omega_f}{2}$, $k_I = \frac{1}{8T_F^2} = \frac{\omega_f^2}{8}$. To include the necessary normalization (see (A.5) and Remark 4.1), the controller parameter are modified to $k_{P,\text{norm}} := \frac{1}{2T_F\varkappa} = \frac{\omega_f}{2\varkappa}$, $k_{I,\text{norm}} := \frac{1}{8T_F^2\varkappa} = \frac{\omega_f^2}{8\varkappa}$ with normalization factor $\varkappa$. This factor has to be chosen according to the knowledge of the turbine and the expected fault (see Remark 4.1). The PI controller of the PLL is finally given by

$$\left.\begin{aligned} v_{\text{LF}}^\bullet(t) &= k_{P,\text{norm}}\bar{v}^{q,\bullet}(t) + k_{I,\text{norm}}\xi_i(t) \\ \tfrac{\mathrm{d}}{\mathrm{d}t}\xi_i(t) &= \bar{v}^{q,\bullet}(t), \qquad \xi_i(0) = 0. \end{aligned}\right\} \tag{23}$$

5. Simulation results

To demonstrate the functionality of the proposed detection system, simulations are conducted. Figure 5 illustrates the overall idea of the torque deviation detection system. Based on the observed turbine torque $\hat{m}_T$ and the computed (ideal) aerodynamical turbine torque $\hat{m}_{T,\text{ideal}}$ (optional), a deviation torque $\hat{m}_{T,\text{dev}}$ is calculated. This deviation torque is analysed by several PLLs for torque oscillations at the respective multiples r of the turbine rotational speed $r\omega_T$. Is the amplitude below a certain threshold, then there is no fault at the respective multiple.

5.1. Simulation scenario

Figure 5 illustrates the simulation scenario. The simulation parameters are given in Tab. 1. For the evaluation of the proposed torque deviation detection system, realistic wind data from the FINO1-platform[2] is used.

There are in total four experiments, that are discussed in the following:

[2] The wind data was measured at the research platform FINO1 (geographical coordinates: $54^\circ\ 00'\ 53,5''N$, $06^\circ\ 35'\ 15,5''E$) on the 24$^{\text{th}}$ Nov. 2012 between 11:50-12:00. The values were saved with a 0.1 s resolution.

Table 1: *System parameters for simulations unless otherwise stated.*

description	symbols & values
implementation	
solver (fixed-step)	Runge-Kutta (ode4)
fixed-step size	$h = 0.1 \cdot 10^{-3}\,\mathrm{s}$
turbine	
turbine inertia	$\Theta_T = 8.6 \cdot 10^6\,\mathrm{kg\,m^2}$
turbine damping	$d_T = 0\,\frac{\mathrm{N\,m\,s}}{\mathrm{rad}}$
rotor radius	$r_T = 40\,\mathrm{m}$
power coefficient	$c_P(\lambda,\beta) = c_{P,2}(\lambda,\beta)$ as in [24]
minimal turbine speed	$\omega_{T,\min} = 0.691\,\frac{\mathrm{rad}}{\mathrm{s}}$
periodicity of deviation	$r = 3$
flexible shaft	
shaft stiffness	$c_S = 2.36 \cdot 10^9\,\frac{\mathrm{N\,m}}{\mathrm{rad}}$
shaft damping	$d_S = 1.35 \cdot 10^7\,\frac{\mathrm{N\,m\,s}}{\mathrm{rad}}$
gear box	
gear box inertia	$\Theta_{Gb} = 0\,\mathrm{kg\,m^2}$
gear box damping	$d_{Gb} = 0\,\frac{\mathrm{N\,m\,s}}{\mathrm{rad}}$
gear box relation	$g_r = 100$

description	symbols & values
environment	
air density	$\rho = 1.293\,\frac{\mathrm{kg}}{\mathrm{m^3}}$
machine	
machine inertia	$\Theta_M = 150\,\mathrm{kg\,m^2}$
machine damping	$d_M = 0\,\frac{\mathrm{N\,m\,s}}{\mathrm{rad}}$
disturbance observer	
weighting matrix	$\boldsymbol{Q} = \mathrm{diag}(1,1,1,1)$
weighting matrix	$\boldsymbol{R} = 0.01 \cdot \mathrm{diag}(1,1,1)$
stability margin	$\alpha = 10$
PLL	
filter damping at $\omega_{\min,r}$	$\lvert F_{v^{d/q},\bullet\to\bar{v}^{d/q},\bullet}(j\omega_{\min,r})\rvert_{\mathrm{dB}} = -30\,\mathrm{dB}$
normalization factor	$\varkappa = 1 \cdot 10^4$
controller	
pitch angle	$\beta = 0°$
machine torque	$m_M(t) = -k_P^\star g_r^2 \omega_T(t)^2$ as in [24], [26], [33, Ch. 8]
torque controller gain	$k_P^\star = 0.278\,\mathrm{kg\,m^2}$

- (E_1) Demonstration of system states and disturbance tracking capability of the disturbance observer (10) (as designed in Sect. 3.2) for an artificial wind profile.
- (E_2) Analysis of torque deviation detection using the PLL *without* taking the ideal turbine torque $\hat{m}_{T,\mathrm{ideal}}$ (see upper block in Fig. 5) into account for a realistic wind speed profile.
- (E_3) Analysis of torque deviation detection using the PLL *and* taking the ideal turbine torque $\hat{m}_{T,\mathrm{ideal}}$ (see upper block in Fig. 5) into account for a realistic wind speed profile.
- (E_4) Same experiment as (E_3), but with measurement noise and deviations in the wind speed measurement and an additional torque deviation at $r = 1$.

5.2. Discussion of torque observer (E_1)

Experiment (E_1) investigates the tracking behaviour of the disturbance observer—designed in Sect. 3.2—for an artificial wind profile. Figure 6(a) shows the results. The upper subplot shows the wind speed, that varies between $5\,\frac{\mathrm{m}}{\mathrm{s}}$ and $7\,\frac{\mathrm{m}}{\mathrm{s}}$. The following subplots show the turbine speed ω_T, the machine speed ω_M and the related angle difference $\Delta\varphi_{TM'}$ on the shaft between turbine and machine side and the corresponding estimates of the observer. It can be seen, that the observer tracks the real values fast and accurately. The turbine torque m_T, the observed turbine torque $\hat{m}_T$ and the related negative machine torque $-m'_M = -g_r m_M$ are shown in subplot five. The observed torque follows the turbine torque accurately even after fast torque changes. In the last subplot, the error between turbine torque m_T and observed turbine torque $\hat{m}_T$ is illustrated. The thin spikes at the jumps in the artificial wind speed are due to the resulting sudden torque jumps. But the disturbance observer quickly changes its estimate to the right value. Besides these thin spikes, the estimation error $m_T - \hat{m}_T$ is very small.

Remark 5.1. *Subplot five shows, that the turbine controller is quite slow (in equilibrium m_T and $-m'_M$ are equal). This is a well known issue for the used turbine controller (see Tab. 1) and there are possibilities to overcome this issue while ensuring convergence to the optimal operating point (for partial load conditions, as shown here), e.g. [33, Ch. 8]. But as that issue is not the focus of this work, the topic is not pursued.*

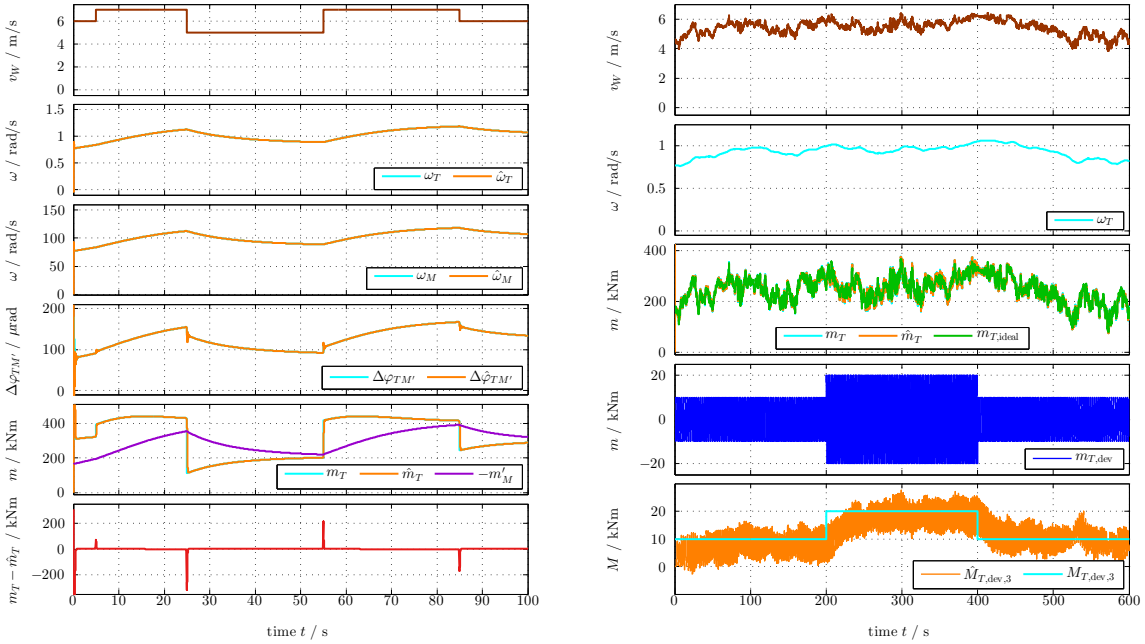

(a) Experiment (E_1): Behaviour of torque observer.

(b) Experiment (E_2): Amplitude detection using only torque observer.

Figure 6: *Simulation results of Experiment (E_1) and Experiment (E_2).*

5.3. Amplitude detection using torque observer (E_2)

From Experiment (E_2) on, a real wind speed profile is used. This experiment is used to investigate the amplitude detection of the torque deviations using *only* the observed turbine torque. The calculation of the ideal aerodynamical wind torque $\hat{m}_{T,\text{ideal}}$ (see upper block in Fig. 5) is *not* used (i.e. $\hat{m}_{T,\text{ideal}} = 0\,\text{N m}$). The wind speed is shown in the upper subplot of Fig. 6(b). The corresponding turbine speed ω_T is shown in the subplot below. The third subplot shows the turbine torque m_T, the observed turbine torque $\hat{m}_T$ and the ideal aerodynamical turbine torque $m_{T,\text{ideal}}$. Recall that, the turbine torque (1) is the sum of the ideal aerodynamical turbine torque and the deviation torque: $m_T(t) = m_{T,\text{ideal}}(t) + m_{T,\text{dev}}(t)$. One can see, that m_T and $\hat{m}_T$ match quite well, the difference between m_T and $m_{T,\text{ideal}}$ is quite substantial, especially between 200 s and 400 s. This is due to the enhanced amplitude of the oscillating deviation torque, as shown in the forth subplot. This can also be seen in the last subplot, where the amplitude $M_{T,\text{dev},3}$ and the observed amplitude $\hat{M}_{T,\text{dev},3}$ are shown. $\hat{M}_{T,\text{dev},3}$ follows $M_{T,\text{dev},3}$ with some time delay and oscillates in a band of about 10 kN m. But a deviation from zero—the value for absence of a torque deviation with $r = 3$—is clearly shown.

Remark 5.2. *The PLL works with the observed turbine torque $\hat{m}_T$ provided by the torque observer. As can be seen, e.g. in the middle subplot in Fig. 6(b), some time is needed between starting the disturbance observer and tracking the turbine torque m_T. For this reason the startup of the PLL algorithm is delayed (here for 2 s).*

5.4. Amplitude detection using torque observer and ideal torque calculation (E_3) & (E_4)

In contrast to Experiment (E_2) (where the observed turbine torque $\hat{m}_T$ is fed to the PLLs), in Experiment (E_3) and Experiment (E_4), the calculated ideal aerodynamical wind torque $\hat{m}_{T,\text{ideal}}$ is used in addition to create a so called residual $\hat{m}_T - \hat{m}_{T,\text{ideal}}$ to feed the PLLs (see Fig. 5). This can improve the detection due to feeding (almost) only the periodic deviation torque to the

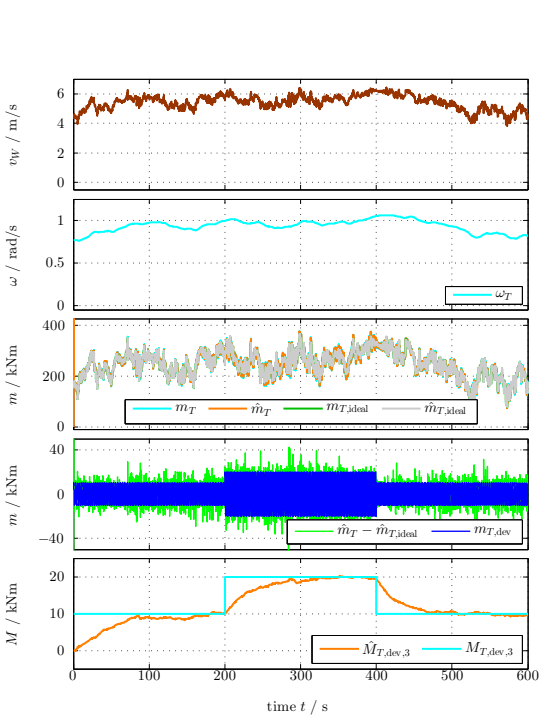

(a) Experiment (E_3): Amplitude detection using torque observer and ideal torque calculation.

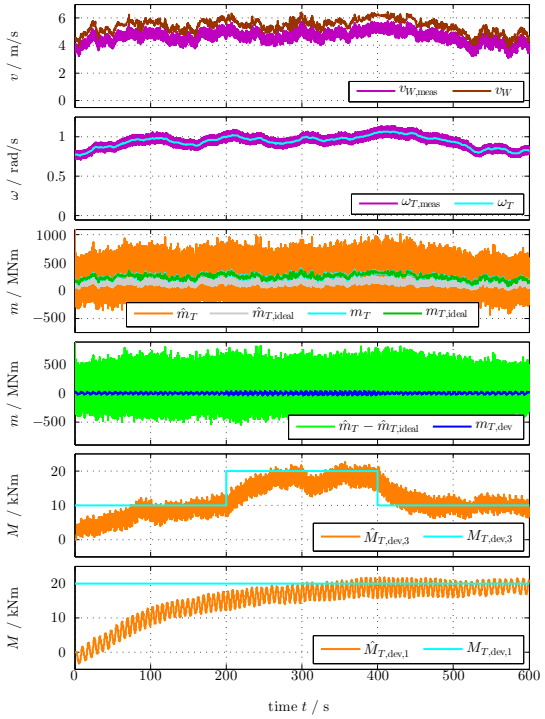

(b) Experiment (E_4): Amplitude detection using torque observer and ideal torque calculation with noisy measurements, deteriorated wind measurement and additional torque deviation.

Figure 7: *Simulation results of Experiment (E_3) and Experiment (E_4).*

PLLs (see (1)).

5.4.1. Discussion of Experiment (E_3) Experiment (E_3) investigates the performance for ideal measurements. This means all measured values equal the real ones. The first and second subplot show the wind speed v_W and the turbine rotational speed ω_T, respectively. Similar to Experiment (E_2), the third subplot shows m_T, $\hat{m}_T$ and $m_{T,\text{ideal}}$. In Fig. 7(a), the signal $\hat{m}_{T,\text{ideal}}$ is added to the subplot. It can be seen, that $\hat{m}_{T,\text{ideal}}$ equals $m_{T,\text{ideal}}$ (which is reasonable due to the ideal measurement). Subplot four shows the torque deviation $m_{T,\text{dev}}$ and the residual $\hat{m}_T - \hat{m}_{T,\text{ideal}}$. The residual deviates slightly from $m_{T,\text{dev}}$ due to the deviation of m_T and $\hat{m}_T$, cf. (1). In the last subplot $M_{T,\text{dev},3}$ and $\hat{M}_{T,\text{dev},3}$ are shown. Compared to Experiment (E_2), the dynamics of the observed deviation amplitude $\hat{M}_{T,\text{dev},3}$ remains the same, but the noise (as shown in the last subplot in Fig. 6(b)) is removed. This is plausible, because of the absence of the (almost) dc-value $m_{T,\text{ideal}}$ in the signal fed into the PLL, that causes oscillation in $\boldsymbol{v}^{dq,\bullet}$ (recall Sect. 4.2.1).

5.4.2. Discussion of Experiment (E_4) Experiment (E_4) is identical to Experiment (E_3) except the following changes:

- The measurements $\omega_{T,\text{meas}}$, $\omega_{M,\text{meas}}$ and $\Delta\varphi_{TM',\text{meas}}$ are affected by noise with an amplitude of 5 % of the respective values (i.e. $\gamma_{\text{meas}}(t) := \gamma(t) + 0.05\gamma(t) \cdot \textsc{WhiteNoise}$ where $\gamma \in \{\omega_T, \omega_M, \Delta\varphi_{TM'}\}$).
- The wind speed measurement is erroneous (the measured value is too small) and affected by noise $v_{W,\text{meas}}(t) := 0.85(v_W(t) + 0.05 \cdot v_W(t) \cdot \textsc{WhiteNoise})$

- A torque deviation for $r = 1$ is added to investigate the capability of the torque deviation system to distinguish between oscillations with different multiples of ω_T. An additional PLL is designed according to the rules given in Sect. 4.2.
- At 300 s, the angle $\varphi_{T,\mathrm{dev},3}$ is increased by $\frac{\pi}{4}$ (to investigate the behaviour of the PLL for jumps in the deviation angle).

Figure 7(b) shows the simulation results. The upper subplot shows the wind speed v_W and the—reduced and noisy—measured wind speed $v_{W,\mathrm{meas}}$. In the second subplot, the turbine rotational speed ω_T and its measured value $\omega_{T,\mathrm{meas}}$ are shown. The noise in the measured value is obvious. Subplot three shows the torques $\hat{m}_T$, $\hat{m}_{T,\mathrm{ideal}}$, m_T and $m_{T,\mathrm{ideal}}$. One can clearly see the noise in the observed torque $\hat{m}_T$. The amplitude of the noise is significantly higher than the actual value of the torque m_T. Another fact is, that the calculated ideal turbine torque $\hat{m}_{T,\mathrm{ideal}}$ is smaller and has more noise than $m_{T,\mathrm{ideal}}$. This is explainable due to the deviations in $v_{W,\mathrm{meas}}$. According to the properties of $\hat{m}_T$ and $\hat{m}_{T,\mathrm{ideal}}$, the residual $\hat{m}_T - \hat{m}_{T,\mathrm{ideal}}$ is very noisy and not symmetrical to the x-axis, as shown in subplot four. A similarity between the residual and $m_{T,\mathrm{dev}}$ can hardly be seen. The fifth subplot shows the amplitude $M_{T,\mathrm{dev},3}$ of the deviation signal and the observed value $\hat{M}_{T,\mathrm{dev},3}$. The dynamic of the observer is identical to Experiment (E_2) and Experiment (E_3). But compared to Experiment (E_2), the band of oscillation is reduced by approximately 5 kN m. So it can be seen, that even with noisy measurements and errors in the wind speed measurement, the amplitude of the torque deviation can be detected. In addition, the usage of the calculated ideal torque $\hat{m}_{T,\mathrm{ideal}}$—even for noisy and erroneous wind measurements—improves the signal quality of the detected amplitude. One reason for this is the reduction of the (almost) dc-value $m_{T,\mathrm{ideal}}$ in the signal fed to the PLL. The change in the angle $\varphi_{T,\mathrm{dev},3}$ at 300 s causes a deviation between $M_{T,\mathrm{dev},3}$ and $\hat{M}_{T,\mathrm{dev},3}$, that is corrected by the PLL after about 50 s. The last plot shows the output $\hat{M}_{T,\mathrm{dev},1}$ of the PLL designed for $r = 1$ and compares it with the amplitude $M_{T,\mathrm{dev},1}$ of the deviation. It can be seen, that the tracking behaviour of the PLL for $r = 1$ is slower than that of the PLL for $r = 3$. This is due to the reduced frequency of the deviation and the resulting design of the PLL parameters. But the PLL tracks the amplitude $M_{T,\mathrm{dev},1}$ of the deviation. This experiment shows, that the PLL approach for detecting torque deviations works in presence of (a) measurement noise, (b) measurement errors in the wind speed, (c) phase changes in the deviation angle and (d) for deviations with different periodicities at the same time.

6. Discussion and Conclusion

This paper discussed the detection of rotational periodic torque deviations in variable speed wind turbine systems. For that a turbine torque disturbance observer was designed. The observer is based on a two-mass model of the turbine drive train. Assuming known model parameters, a LQR approach was used to compute the observer gain. To compute a residual between fault-free (ideal, without torque deviation) turbine torque and real turbine torque (with torque deviation), the aerodynamical torque is calculated, based on the power curve of the turbine and the measurement of the wind speed. To analyse the time series of the resulting torque, a phase-locked loop (PLL) was designed. The working principle of a single-phase PLL with a quadrature-signal-generator (QSG) based on the Park transform was investigated. Additionally, guidelines for filter tuning and controller design were presented.

Simulation results illustrated the functionality and capability of the torque observer and compared the deviation detection performance for different torque signals by the PLL. Without the usage of the calculated aerodynamical torque, the amplitude of the deviation can be detected but fluctuates. Using the aerodynamical torque, the amplitude can be detected without noise in the signal. Furthermore, even with noisy measurements, wrong wind measurement and torque deviations at different periodicities, these deviations can be detected by the proposed approach

using the residual of observed turbine torque and calculated aerodynamical torque.
The simulations are a first proof of concept. But for assessment of the applicability of this approach in a real wind turbine, precise knowledge of the relevant deviations, their amplitudes, their periodicity and the disturbance components in the measured signals of a specific wind turbine are essential. Unfortunately the authors do not have access to that kind of information. This wide range of necessary information of a specific wind turbine is probably only known to the manufacturer. As a next step, the testing with real turbine data would be a good possibility to further investigate suitability of this approach for fault detection.
The approach using a PLL for signal analysis has some limitations. The periodicity for each fault has to be known a priori, to design a suitable PLL. Additionally, for each possible fault—as long as the periodicity is different—a separate PLL is needed. The first point might be an issue, if knowledge of the turbine is not available, but as stated before, the wind turbine manufacturer should be aware of the relevant periodicities. The latter might be tedious but due to the simplicity of the proposed PLL should not be a problem regarding implementation.

Acknowledgement
The authors are deeply grateful to the FINO-Project (BMU, PTJ, BSH, DEWI GmbH) for providing the wind data used for the simulation. This project has received funding from the Bavarian Ministry for Education, Culture, Science, and Art.

References

[1] W. Yang, P. J. Tavner, C. J. Crabtree, Y. Feng, and Y. Qiu, "Wind turbine condition monitoring: technical and commercial challenges," *Wind Energy*, vol. 17, no. 5, pp. 673–693, 2014.
[2] C. J. Crabtree, D. Zappalá, and P. J. Tavner, "Survey of commercially available condition monitoring systems for wind turbines." Durham University School of Engineering and Computing Sciences and the SUPERGEN Wind Energy Technologies Consortium, Tech. Rep., 2014.
[3] W. Qiao, "Recovery act: Online nonintrusive condition monitoring and fault detection for wind turbines," University of Nebraska - Lincoln, Tech. Rep., 2012.
[4] X. Gong and W. Qiao, "Imbalance fault detection of direct-drive wind turbines using generator current signals," *IEEE Transactions on Energy Conversion*, vol. 27, no. 2, pp. 468–476, June 2012.
[5] W. Q. Jeffries, J. A. Chambers, and D. G. Infield, "Experience with bicoherence of electrical power for condition monitoring of wind turbine blades," *IEE Proceedings - Vision, Image and Signal Processing*, vol. 145, no. 3, pp. 141–148, Jun 1998.
[6] D. J. Gardels, W. Qiao, and X. Gong, "Simulation studies on imbalance faults of wind turbines," in *IEEE PES General Meeting*, July 2010, pp. 1–5.
[7] S. Cacciola, I. M. Agud, and C. Bottasso, "Detection of rotor imbalance, including root cause, severity and location," *Journal of Physics: Conference Series*, vol. 753, no. 7, p. 072003, 2016.
[8] R. Ramlau and J. Niebsch, "Imbalance estimation without test masses for wind turbines," *Journal of Solar Energy Engineering*, vol. 131, no. 1, p. 011010, 2009.
[9] R. Fadaeinedjad, G. Moschopoulos, and M. Moallem, "The impact of tower shadow, yaw error, and wind shears on power quality in a wind-diesel system," *IEEE Transactions on Energy Conversion*, vol. 24, no. 1, pp. 102–111, March 2009.
[10] D. Lu, X. Gong, and W. Qiao, "Current-based diagnosis for gear tooth breaks in wind turbine gearboxes," in *2012 IEEE Energy Conversion Congress and Exposition (ECCE)*, Sept 2012, pp. 3780–3786.
[11] S. Chakkor, B. Bostafa, and H. Abderrahmane, "Performance analysis of fault detection in wind turbine generator based on high-resolution frequency estimation methods," *International Journal of Advanced Computer Science and Applications (IJACSA)*, vol. 5, no. 4, 2014.
[12] E. Al-Ahmar, M. Benbouzid, and S. Turri, "Wind energy conversion systems fault diagnosis using wavelet analysis," *International Review of Electrical Engineering*, vol. 3, no. 4, pp. 646–652, 2008.
[13] Y. Amirat, V. Choqueuse, and M. E. H. Benbouzid, "Wind turbines condition monitoring and fault diagnosis using generator current amplitude demodulation," in *2010 IEEE International Energy Conference and Exhibition (EnergyCon)*, Dec 2010, pp. 310–315.
[14] N. Perišić, P. H. Kirkegaard, and B. J. Pedersen, "Cost-effective shaft torque observer for condition monitoring of wind turbines," *Wind Energy*, vol. 18, no. 1, pp. 1–19, 2015.
[15] M. L. Corradini, G. Ippoliti, and G. Orlando, "Robust control of variable-speed wind turbines based on

an aerodynamic torque observer," *IEEE Transactions on Control Systems Technology*, vol. 21, no. 4, pp. 1199–1206, July 2013.
[16] T. Puleva and J. Osusky, "Wind turbine power control based on aero dynamical torque estimation," in *2016 Cybernetics Informatics (K I)*, Feb 2016, pp. 1–6.
[17] O. Barambones and J. M. G. de Durana, "Adaptive sliding mode control strategy for a wind turbine systems using a hosm wind torque observer," in *2016 IEEE International Energy Conference (ENERGYCON)*, April 2016, pp. 1–6.
[18] I. Hochmannová, F. F. Wamba, and J. Liška, "Anwendung von Zeit-Frequenz-Methoden für drehzahlvariable und niedertourige Windenergieanlagen," in *VDI Berichte*, no. 2200, 2013, pp. 31–46.
[19] F. P. García Márquez, A. M. Tobias, J. M. Pinar Pérez, and M. Papaelias, "Condition monitoring of wind turbines: Techniques and methods," *Renewable Energy*, vol. 46, pp. 169–178, 2012.
[20] W. Yang, P. Tavner, and M. Wilkinson, "Condition monitoring and fault diagnosis of a wind turbine synchronous generator drive train," *Renewable Power Generation, IET*, vol. 3, no. 1, pp. 1–11, 2009.
[21] W. Yang, P. J. Tavner, and M. Wilkinson, "Wind turbine condition monitoring and fault diagnosis using both mechanical and electrical signatures," in *IEEE/ASME International Conference on Advanced Intelligent Mechatronics, 2008. AIM 2008.* IEEE, 2008, pp. 1296–1301.
[22] W. Yang, P. J. Tavner, C. J. Crabtree, and M. Wilkinson, "Cost-effective condition monitoring for wind turbines," *IEEE Transactions on Industrial Electronics*, vol. 57, no. 1, pp. 263–271, 2010.
[23] B. Lu, Y. Li, X. Wu, and Z. Yang, "A review of recent advances in wind turbine condition monitoring and fault diagnosis," in *Power Electronics and Machines in Wind Applications, 2009. PEMWA 2009. IEEE*, June 2009, pp. 1–7.
[24] C. Dirscherl, C. Hackl, and K. Schechner, "Modellierung und Regelung von modernen Windkraftanlagen: Eine Einführung *(available at the authors upon request)*," in *Elektrische Antriebe – Regelung von Antriebssystemen*, D. Schröder, Ed. Springer-Verlag, 2015, ch. 24, pp. 1540–1614.
[25] C. M. Hackl, *Non-identifier based adaptive control in mechatronics: Theory and Application*, ser. Lecture Notes in Control and Information Sciences. Berlin: Springer International Publishing, 2017, no. 466. [Online]. Available: http://www.springer.com/de/book/9783319550343
[26] C. Hackl and K. Schechner, "Non-ideal feedforward torque control of wind turbines: Impacts on annual energy production & gross earnings," *Journal of Physics: Conference Series*, vol. 753, no. 11, p. 112010, 2016. [Online]. Available: http://stacks.iop.org/1742-6596/753/i=11/a=112010
[27] G. Ludyk, *Theoretische Regelungstechnik 2.* Springer-Verlag, 1995.
[28] O. Föllinger, *Regelungstechnik*, 10th ed. Heidelberg: Hüthig Verlag, 2008.
[29] D. Abramovitch, "Phase-locked loops: A control centric tutorial," in *Proceedings of the 2002 American Control Conference (IEEE Cat. No. CH37301)*, vol. 1. IEEE, 2002, pp. 1–15.
[30] S. Golestan, M. Monfared, F. D. Freijedo, and J. M. Guerrero, "Dynamics assessment of advanced single-phase PLL structures," *IEEE Transactions on Industrial Electronics*, vol. 60, no. 6, pp. 2167–2177, June 2013.
[31] R. Teodorescu, M. Liserre, and P. Rodríguez, *Grid Converters for Photovoltaic and Wind Power Systems.* Chichester, United Kingdom: John Wiley & Sons, Ltd., 2011.
[32] D. Schröder, *Elektrische Antriebe - Regelung von Antriebssystemen*, 4th ed. Berlin Heidelberg: Springer-Verlag, 2015.
[33] T. Burton, D. Sharpe, N. Jenkins, and E. Bossanyi, *Wind energy handbook*, 2nd ed. John Wiley & Sons, 2011.